

Article

A Clock Transition in the Cr₇Mn Molecular Nanomagnet

Charles A. Collett¹, Kai-Isaak Ellers¹, Nicholas Russo^{2,†} , Kevin R. Kittilstved² , Grigore A. Timco³ , Richard E. P. Winpenny³ and Jonathan R. Friedman^{1,*}

¹ Department of Physics and Astronomy, Amherst College, Amherst, MA 01002, USA; ccollett@amherst.edu (C.A.C.); kellers19@amherst.edu (K.I.-E.)

² Department of Chemistry, University of Massachusetts, Amherst, MA 01003, USA; nzs@bu.edu (N.R.); kittilstved@chem.umass.edu (K.R.K.)

³ School of Chemistry, The University of Manchester, Manchester M13 9PL, UK; Grigore.Timco@manchester.ac.uk (G.A.T.); Richard.Winpenny@manchester.ac.uk (R.E.P.W.)

* Correspondence: jrfriedman@amherst.edu

† Current address: Department of Physics, Boston University, Boston, MA 02215, USA.

Received: 21 November 2018; Accepted: 10 January 2019; Published: 14 January 2019



Abstract: A viable qubit must have a long coherence time T_2 . In molecular nanomagnets, T_2 is often limited at low temperatures by the presence of dipole and hyperfine interactions, which are often mitigated through sample dilution, chemical engineering and isotope substitution in synthesis. Atomic-clock transitions offer another route to reducing decoherence from environmental fields by reducing the effective susceptibility of the working transition to field fluctuations. The Cr₇Mn molecular nanomagnet, a heterometallic ring, features a clock transition at zero field. Both continuous-wave and spin-echo electron-spin resonance experiments on Cr₇Mn samples, diluted via co-crystallization, show evidence of the effects of the clock transition with a maximum $T_2 \sim 390$ ns at 1.8 K. We discuss improvements to the experiment that may increase T_2 further.

Keywords: electron spin resonance; clock transition; molecular nanomagnet

1. Introduction

The fundamental building block of a quantum computer is a qubit, a two-level system that can be in a superposition of the two levels. There are a wide variety of physical systems that can be used as qubits. Molecular nanomagnets (MNMs) have received significant attention due to their possible utility as spin qubits [1–3]. MNMs can be chemically engineered, allowing the design of samples with desired characteristics, and manipulation and control of the spin state can be performed through electron-spin resonance (ESR) [4–6]. The ideal qubit would feature a quantum state with a long lifetime that is able to be precisely controlled and measured, as well as coupled to an array of other such qubits in a controllable manner. The engineerability of MNMs affords the ability to couple multiple MNMs together to create multi-qubit systems [4,7–9]. In order for such systems to be viable qubits, the coherence time T_2 needs to be long compared to the time required for quantum gates. Here, we present experimental results showing an enhancement of T_2 in the Cr₇Mn MNM through the use of a so-called atomic-clock transition.

Cr₇Mn [(CH₃)₂NH₂][Cr₇MnF₈((CH₃)₃CCOO)₁₆] is a paramagnetic ring, shown in Figure 1b [10,11]. At low-temperature, it has a ground-state spin of $S = 1$ that can be described by the spin Hamiltonian

$$\mathcal{H} = -DS_z^2 + E(S_x^2 - S_y^2) - g\mu_B \vec{B} \cdot \vec{S}, \quad (1)$$

where $D = 21$ GHz, $E = 1.9$ GHz, $g = 1.96$ is the Landé g -factor and μ_B is the Bohr magneton. The D term describes the longitudinal anisotropy of the molecule, and gives the $|\pm 1\rangle$ states a lower energy than the $|0\rangle$ state, while the E term describes the transverse anisotropy that breaks the zero-field degeneracy of the $|\pm 1\rangle$ states by mixing them, as shown at the left edge of Figure 1a. Due to this mixing, the two lowest-energy levels are the superpositions $|\pm\rangle = (|+1\rangle \pm |-1\rangle)/\sqrt{2}$, forming an avoided crossing at zero field with a “tunnel splitting” energy $\Delta = 2E$. The application of a magnetic field along the easy axis, B_z , results in an additional Zeeman splitting of the two lowest energy levels with no change in the energy of the $|0\rangle$ state, as shown in Figure 1a.

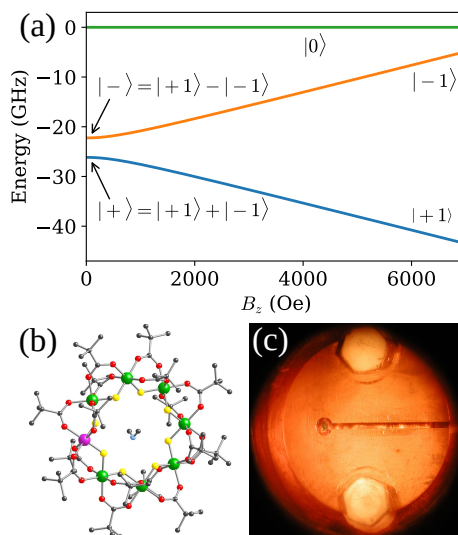


Figure 1. (a) energy-level diagram for a Cr₇Mn molecule, showing the zero-field avoided crossing between $|m = \pm 1\rangle$ states, creating the $|\pm\rangle$ clock states; (b) molecular structure of Cr₇Mn; (c) picture of a loop-gap resonator with a Cr₇Mn sample in the loop.

Near the zero-field avoided crossing, the leading-order dependence of the tunnel splitting on the magnetic field is quadratic: $\Delta \propto B_z^2$. Because of this dependence, at zero field, the splitting is, to first order, insensitive to field fluctuations: $\left. \frac{d\Delta}{dB_z} \right|_{B_z=0} = 0$. This type of transition is known as an atomic-clock, or just clock, transition, based on its use in the atomic clock community to achieve frequency stability [12]. A recent experiment in a Ho-based MNM has shown that clock transitions produce significant increases in quantum coherence times [13], as the main source of decoherence at low temperatures is dipolar interactions with neighboring spins, whose fluctuations cause changes in the local magnetic field seen by the central spin [14]. At a clock transition, the effect of these fluctuations is suppressed, leading to the observed increase in coherence times. Here, we show evidence of the effect of a clock transition in Cr₇Mn.

2. Results

We use ESR to probe and control the state of this molecule, coupling radiation to our samples with custom loop-gap resonators (LGRs). LGRs concentrate the oscillating magnetic field in a narrow region, producing high filling factors [15].

2.1. CW Experiments

For our continuous-wave (CW) measurements, we placed a crystal of Cr₇Mn in the loop of an LGR tuned to 4.00 GHz, near the zero-field tunnel splitting where the effect of the clock transition is strongest. We then cooled it to 1.8 K and swept a magnetic field applied along the easy axis while measuring

$Q = \nu / \Delta\nu$ of the resonator, where ν is the resonance frequency and $\Delta\nu$ is the full width at half maximum of the resonance peak. When the sample is on resonance with the resonator, it absorbs energy from the radio-frequency (RF) magnetic field in the loop, increasing the loading and reducing the Q of the resonator. As such, we measure the coupling of the sample to the resonator by reduction in Q .

Figure 2a shows measured values of Q as a function of magnetic field. The lowest (purple) trace corresponds to an input power of -20 dBm, while our highest power of 0 dBm is red, with intermediate powers designated with intermediate spectral colors. The slight dip around 500 Oe is due to an impurity unrelated to the sample. At the lowest powers, we see a broad dip in Q around zero field, as expected for a transition between the two levels in the avoided crossing (cf. Figure 1a); the width of the peak is due to significant inhomogeneous broadening in the sample, as well as the fact that the transition frequency depends quadratically on field near the clock transition. As we increased the power, Q also increased over the entire field range, but with a pronounced shape change near zero field. An increase in Q indicates a decrease in the coupling between sample and resonator, so this effect shows that as power increases the sample is decoupling from the resonator preferentially around zero field. We have also done experiments at lower powers, down to -55 dBm (not shown), with results indistinguishable from the -20 dBm trace. This shows that the decoupling is a nonlinear effect, associated with the interaction between the sample and the resonator and not a feature of the resonator itself.

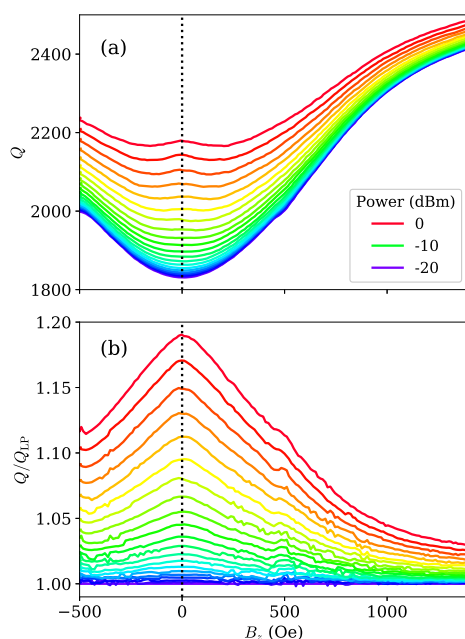


Figure 2. (a) resonator Q vs. applied magnetic field at 4.00 GHz and powers from -20 to 0 dBm; (b) resonator Q divided by the Q at -20 dBm to emphasize the decoupling effect. The sharp peak around zero field suggests that this decoupling is associated with the clock transition.

To isolate this power dependence, we divided the -20 dBm Q data from the higher power Q data, shown in Figure 2b as Q/Q_{LP} . The resulting “decoupling peak” is nearly triangular, being sharply peaked at zero field; the shape change seen in the raw Q data is the result of this triangular decoupling peak superimposed with the smoother resonance dip. This plot shows that the decoupling has a smooth, monotonic power dependence and is strongest near zero field. The reduction in coupling with increasing power is consistent with saturation of the transition, but the shape of the decoupling peak suggests that the saturation is being strongly enhanced near zero field. As the main feature at zero field is the avoided

crossing, we propose that this decoupling peak demonstrates saturation enhanced by the increase in T_2 produced by the clock transition [16,17].

2.2. Spin Echo Experiments

While our CW measurements suggest the existence of a clock transition in Cr_7Mn , to verify it, we directly measured T_2 using a Hahn echo sequence. Using the same Cr_7Mn crystal from our CW experiments, we were unable to see any echo, indicating that T_2 is too short for our apparatus to detect because of strong dipolar interactions between molecules within the crystal. To increase T_2 by increasing the average distance between molecular spins, we diluted the Cr_7Mn molecules through co-crystallization with an isostructural diamagnetic analogue, $[(\text{CH}_3)_2\text{NH}_2][\text{Ga}_7\text{ZnF}_8((\text{CH}_3)_3\text{CCOO})_{16}]$ (“ Ga_7Zn ”) [18,19]. The resulting solid solution crystal has the advantage of preserving the orientational order of the molecules. Previous measurements of dilute Cr_7Mn suggest a maximum coherence time of ~ 600 ns at 2 K in the dilute limit, increasing to ~ 4 μs for deuterated samples [20].

With our 10% and 0.5% samples, T_2 was long enough to be measurable. To verify that we were observing a spin-echo signal, we performed nutation measurements by changing the length of the extra pulse described in the Methods section. Some results for a 10% sample, background-subtracted using the high field method described in Methods, are plotted in Figure 3, showing the expected Rabi oscillations. We used these results to determine the starting duration of our $\pi/2$ and π pulses, which we then tuned to maximize our signal.

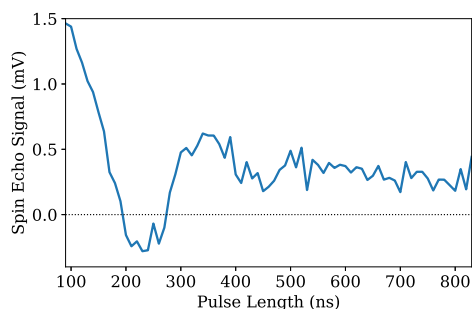


Figure 3. Spin echo signal as a function of the length of the extra pulse, at 4.43 GHz and 0 Oe. The resulting Rabi oscillations confirm that our signal comes from spin echo. The offset is an artifact of our background-subtraction method.

Spin echo results for a 10%-dilution sample at several different delay times τ , background subtracted using the third-pulse method described in Methods, are shown in Figure 4a, with each trace offset in time so the echoes occur at the same place in the plot. We measured T_2 by plotting the echo signal area vs. 2τ , as shown in Figure 4b, and fitting to an exponential decay function to obtain $T_2 = 380$ ns at an applied field of 20 Oe for the 10% sample. Surprisingly, our measured T_2 value for the 0.5% sample was only slightly higher, $T_2 = 390$ ns at 20 Oe. Thus, different dilution levels did not produce the expected increase in T_2 , instead yielding roughly constant coherence times.

As we are near neither the dilute limit nor the expected maximum T_2 , we suspect that the co-crystallization method is limiting our value of T_2 somehow, either through spectral diffusion produced by spins in the Ga_7Zn , interaction with the nuclear spin of Ga, or acoustic phonons in the crystal. Alternatively, the Cr_7Mn may be aggregating in the co-crystallization, limiting the effect of dilution. The presence of an echo signal for the dilute samples shows that dilution is having some effect, but the lack of change in T_2 indicates that the effect of this method of dilution for this molecule has saturated by the time we have reached 10% dilution. This limitation should be specific to our co-crystallization method,

and we expect the previously-used method of diluting Cr₇Mn by dissolving it in toluene should be more effective, as that technique has yielded larger values of T_2 [20].

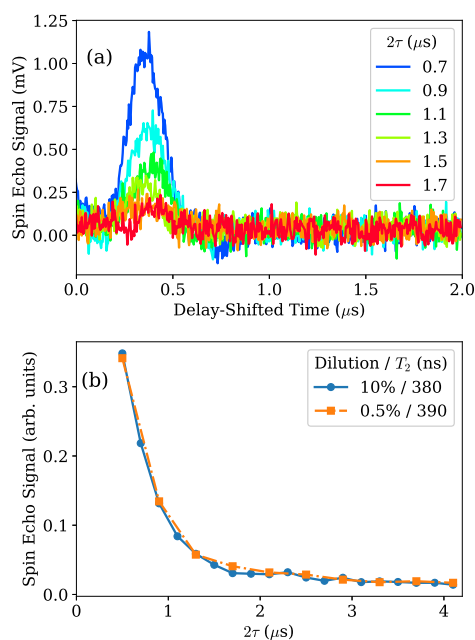


Figure 4. (a) background-subtracted spin echo signal at various delay times 2τ , at 4.43 GHz and 20 Oe. The time axis has been shifted such that every echo occurs at the same effective time; (b) spin echo signal area as a function of the delay time 2τ for 10% (blue circles) and 0.5% (orange squares) samples. The lines connecting datapoints are guides to the eye.

We performed spin echo measurements over a range of fields in order to find the field dependence. Figure 5 shows measured T_2 as a function of field for samples of both dilutions. The data exhibit a significant peak in T_2 near zero field, as we would expect for a clock transition. This peak appears slightly away from zero field due to the remnant field of our superconducting magnet, such that an applied field of ~ 20 Oe is required to zero the field at the sample. This peak corroborates the hypothesis that the avoided crossing in Cr₇Mn acts as a clock transition, agreeing with our CW results.

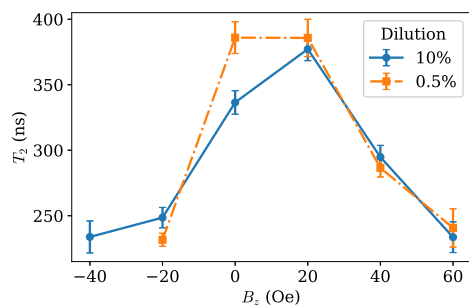


Figure 5. T_2 as a function of applied field for 10% (blue circles, at 4.43 GHz) and 0.5% (orange squares, at 4.50 GHz) samples. The apparent offset of the peaks from 0 Oe is due to remnant field in our magnet. The lines connecting datapoints are guides to the eye.

3. Conclusions

We have presented here results from both CW and pulsed experiments exploring a possible clock transition in the MNM Cr₇Mn. The CW results suggest the presence of a clock transition through a field-dependent saturation peak at higher radiation powers, centered around zero field. These results are corroborated by spin echo experiments, which also show a peak in T_2 around zero field, where we expect the effect of the clock transition to be strongest. This agreement shows that CW saturation experiments can be useful in locating clock transitions and characterizing the field dependence of coherence times.

In addition, we found that our method of dilution via co-crystallization is ineffective past a fairly low level of dilution. This restriction in dilution limited our ability to characterize the clock transition. Experiments to work around this restriction by creating dilute solutions of Cr₇Mn dissolved in toluene and measuring their properties are ongoing. Characterization of such samples will allow us to determine if the field dependence of T_2 exhibits the expected significant enhancement near zero field, the center of the avoided crossing.

4. Materials and Methods

We used custom loop-gap resonators for our ESR experiments, and tuned their frequencies by inserting a dielectric into the gap. Our sample sat in the loop of the resonator, as shown in Figure 1c, and we coupled radiation into the system through antennae above the loop and/or the gap. Continuous wave measurements were done using a vector network analyzer (KeySight E5063A, Santa Rosa, CA, USA). Pulsed experiments were performed using a homemade pulsed-ESR spectrometer, configured to perform a Hahn echo sequence. Two RF pulses were sent to the resonator, the first with a duration such that it tipped the spin state by an angle of $\pi/2$, followed after a time τ by a second pulse which tipped the state by an angle of π , producing a “spin echo” a time τ after the second pulse, resulting in the sequence $\pi/2 - \tau - \pi - \tau$ -echo. Fitting the dependence of the echo signal on 2τ to an exponential decay gives a time constant of T_2 . We also performed background subtraction in one of two ways. For our preliminary experiments, we took data at a low field and a much higher field, where the sample is no longer coupled to the resonator; subtracting the two signals removes the background. For our T_2 experiments, we alternated sending in a π pulse several μ s before the $\pi/2$ pulse. This extra pulse inverts the echo; subtracting signals with this extra pulse from signals without the extra pulse removes the background while effectively doubling our echo signal.

Synthesis of Cr₇Mn [21] and Ga₇Zn [19] was done following published procedures. To create the dilute solution, (Me₂NH₂)[Ga₇ZnF₈(O₂CtBu)₁₆] and (Me₂NH₂)[Cr₇MnF₈(O₂CtBu)₁₆] were dissolved in anhydrous toluene while stirring at 100 °C for 10 min under an N₂ atmosphere. The clear solution was cooled to ambient temperature and left undisturbed. Well-shaped green crystals were collected after several days. We produced samples volumetrically diluted to 10% and 0.5% Cr₇Mn (green) in Ga₇Zn (clear/white). The dilution had the qualitative effect of markedly decreasing the green tint of the crystals with increased dilution.

Author Contributions: Conceptualization, C.A.C. and J.R.F.; Methodology, C.A.C. and J.R.F.; Software, C.A.C. and K.-I.E.; Validation, C.A.C., K.-I.E. and J.R.F.; Formal Analysis, C.A.C. and K.-I.E.; Investigation, C.A.C. and K.-I.E.; Resources, N.R., K.R.K., G.A.T. and R.E.P.W.; Sample Preparation, G.A.T.; Data Curation, C.A.C.; Writing—Original Draft Preparation, C.A.C.; Writing—Review and Editing, C.A.C., K.-I.E., K.R.K. and J.R.F.; Visualization, C.A.C.; Supervision, J.R.F.; Project Administration, J.R.F.; Funding Acquisition, J.R.F.

Funding: This research was funded by the U.S. National Science Foundation under Grant Nos. DMR-1310135 and DMR-1708692 and by the Amherst College Dean of Faculty. The research was also funded by the EPSRC(UK) via an Established Career Fellowship (EP/R011079/1) to R.E.P.W.

Acknowledgments: We thank Gajadhar Joshi, Stephen Hill, Adrian Lupascu, Jonathan Baugh and Miles Blencowe for useful conversations, and Changyun Yoo and Elizabeth Turnbull for preliminary sample characterization work.

Conflicts of Interest: The authors declare no conflict of interest.

Abbreviations

The following abbreviations are used in this manuscript:

MNM	Molecular nanomagnet
ESR	Electron-spin resonance
LGR	Loop-gap resonator
CW	Continuous-wave
RF	Radio frequency

References

1. Leuenberger, M.N.; Loss, D. Quantum computing in molecular magnets. *Nature* **2001**, *410*, 789–793. [[CrossRef](#)] [[PubMed](#)]
2. Tejada, J.; Chudnovsky, E.M.; Del Barco, E.; Hernandez, J.M.; Spiller, T.P. Magnetic qubits as hardware for quantum computers. *Nanotechnology* **2001**, *12*, 181. [[CrossRef](#)]
3. Friedman, J.R.; Sarachik, M.P. Single-Molecule Nanomagnets. *Annu. Rev. Condens. Matter Phys.* **2010**, *1*, 109–128. [[CrossRef](#)]
4. Ardavan, A.; Bowen, A.M.; Fernandez, A.; Fielding, A.J.; Kaminski, D.; Moro, F.; Mury, C.A.; Wise, M.D.; Ruggi, A.; McInnes, E.J.L.; et al. Engineering coherent interactions in molecular nanomagnet dimers. *NPJ Quantum Inf.* **2015**, *1*, 15012. [[CrossRef](#)]
5. Wedge, C.J.; Timco, G.A.; Spielberg, E.T.; George, R.E.; Tuna, F.; Rigby, S.; McInnes, E.J.L.; Winpenny, R.E.P.; Blundell, S.J.; Ardavan, A. Chemical Engineering of Molecular Qubits. *Phys. Rev. Lett.* **2012**, *108*, 107204. [[CrossRef](#)] [[PubMed](#)]
6. Timco, G.A.; Carretta, S.; Troiani, F.; Tuna, F.; Pritchard, R.J.; Mury, C.A.; McInnes, E.J.L.; Ghirri, A.; Candini, A.; Santini, P.; et al. Engineering the coupling between molecular spin qubits by coordination chemistry. *Nat. Nanotechnol.* **2009**, *4*, 173–178. [[CrossRef](#)]
7. Chiesa, A.; Whitehead, G.F.S.; Carretta, S.; Carthy, L.; Timco, G.A.; Teat, S.J.; Amoretti, G.; Pavarini, E.; Winpenny, R.E.P.; Santini, P. Molecular nanomagnets with switchable coupling for quantum simulation. *Sci. Rep.* **2015**, *4*, 7423. [[CrossRef](#)]
8. Timco, G.A.; Faust, T.B.; Tuna, F.; Winpenny, R.E.P. Linking heterometallic rings for quantum information processing and amusement. *Chem. Soc. Rev.* **2011**, *40*, 3067. [[CrossRef](#)]
9. Ferrando-Soria, J.; Moreno Pineda, E.; Chiesa, A.; Fernandez, A.; Magee, S.A.; Carretta, S.; Santini, P.; Vitorica-Yrezabal, I.J.; Tuna, F.; Timco, G.A.; et al. A modular design of molecular qubits to implement universal quantum gates. *Nat. Commun.* **2016**, *7*, 11377. [[CrossRef](#)]
10. Piligkos, S.; Weihe, H.; Bill, E.; Neese, F.; El Mkami, H.; Smith, G.M.; Collison, D.; Rajaraman, G.; Timco, G.A.; Winpenny, R.E.P.; et al. EPR Spectroscopy of a Family of Cr^{III}₇M^{II} (M = Cd, Zn, Mn, Ni) “Wheels”: Studies of Isostructural Compounds with Different Spin Ground States. *Chem. A Eur. J.* **2009**, *15*, 3152–3167. [[CrossRef](#)]
11. Lancaster, T.; Blundell, S.J.; Pratt, F.L.; Franke, I.; Steele, A.J.; Baker, P.J.; Salman, Z.; Baines, C.; Watanabe, I.; Carretta, S.; et al. Relaxation of muon spins in molecular nanomagnets. *Phys. Rev. B* **2010**, *81*, 140409R. [[CrossRef](#)]
12. Bollinger, J.J.; Prestage, J.D.; Itano, W.M.; Wineland, D.J. Laser-Cooled-Atomic Frequency Standard. *Phys. Rev. Lett.* **1985**, *54*, 1000–1003. [[CrossRef](#)] [[PubMed](#)]
13. Shiddiq, M.; Komijani, D.; Duan, Y.; Gaita-Ariño, A.; Coronado, E.; Hill, S. Enhancing coherence in molecular spin qubits via atomic clock transitions. *Nature* **2016**, *531*, 348–351. [[CrossRef](#)] [[PubMed](#)]
14. Takahashi, S.; Tupitsyn, I.S.; van Tol, J.; Beedle, C.C.; Hendrickson, D.N.; Stamp, P.C.E. Decoherence in crystals of quantum molecular magnets. *Nature* **2011**, *476*, 76–79. [[CrossRef](#)] [[PubMed](#)]
15. Froncisz, W.; Hyde, J.S. The loop-gap resonator: A new microwave lumped circuit ESR sample structure. *J. Magn. Reson.* **1982**, *47*, 515–521. [[CrossRef](#)]

16. Portis, A.M. Electronic Structure of F Centers: Saturation of the Electron Spin Resonance. *Phys. Rev.* **1953**, *91*, 1071–1078. [[CrossRef](#)]
17. Castner, T.G., Jr. Saturation of the paramagnetic resonance of a V center. *Phys. Rev.* **1959**, *115*, 1506. [[CrossRef](#)]
18. Henderson, J.J.; Ramsey, C.M.; del Barco, E.; Stamatatos, T.C.; Christou, G. Control of the inhomogeneity degree by magnetic dilution in crystals of antiferromagnetic molecular rings. *Phys. Rev. B* **2008**, *78*, 214413. [[CrossRef](#)]
19. Moro, F.; Kaminski, D.; Tuna, F.; Whitehead, G.F.S.; Timco, G.A.; Collison, D.; Winpenny, R.E.P.; Ardavan, A.; McInnes, E.J.L. Coherent electron spin manipulation in a dilute oriented ensemble of molecular nanomagnets: Pulsed EPR on doped single crystals. *Chem. Commun.* **2013**, *50*, 91–93. [[CrossRef](#)] [[PubMed](#)]
20. Ardavan, A.; Rival, O.; Morton, J.J.L.; Blundell, S.J.; Tyryshkin, A.M.; Timco, G.A.; Winpenny, R.E.P. Will Spin-Relaxation Times in Molecular Magnets Permit Quantum Information Processing? *Phys. Rev. Lett.* **2007**, *98*, 057201. [[CrossRef](#)]
21. Larsen, F.K.; McInnes, E.J.L.; El Mkami, H.; Overgaard, J.; Piligkos, S.; Rajaraman, G.; Rentschler, E.; Smith, A.A.; Smith, G.M.; Boote, V.; et al. Synthesis and Characterization of Heterometallic Cr₇M Wheels. *Angew. Chem. Int. Ed.* **2003**, *42*, 101. [[CrossRef](#)]



© 2019 by the authors. Licensee MDPI, Basel, Switzerland. This article is an open access article distributed under the terms and conditions of the Creative Commons Attribution (CC BY) license (<http://creativecommons.org/licenses/by/4.0/>).